

## LETTER

### Scanning tunneling microscopy of defects in Ag- and Sb-bearing galena

THOMAS G. SHARP

Department of Geology, Arizona State University, Tempe, Arizona 85287, U.S.A.

NAN JIU ZHENG,\* IGNATIUS S. T. TSONG

Department of Physics, Arizona State University, Tempe, Arizona 85287, U.S.A.

PETER R. BUSECK

Departments of Geology and Chemistry, Arizona State University, Tempe, Arizona 85287, U.S.A.

#### ABSTRACT

We have used scanning tunneling microscopy (STM) to investigate defects in Ag- and Sb-bearing galena from Zacatecas, Mexico. Large-area scans produced images of topographic features that formed during cleavage. Pits occur that are from 10 to 300 nm in diameter and >30 nm deep and are surrounded by what appear to be crystal fragments. These pits are interpreted as the remains of diaphorite inclusions that were plucked during cleavage.

Most of our atomic-resolution images have 0.42-nm periodicities, corresponding to the distance between corner and face-centered atoms in the galena structure. This periodicity indicates that only half the atoms are resolved in the images. Defects in surface structure consist of atoms that are laterally displaced from their ideal positions, resulting in kinking of atomic rows that parallel [110]. These defects are unlike any reported in previous STM studies of galena, suggesting that they are unique to the Ag- and Sb-bearing samples. A possible explanation for these local disruptions of the structure is strain caused by grouped substitution of Ag and Sb for Pb.

#### INTRODUCTION

Scanning tunneling microscopy (STM) has been used to image defects on the atomic scale in Ag- and Sb-bearing galena as part of ongoing research using STM (Sharp et al., 1989) and high-resolution transmission electron microscopy (HRTEM) (Sharp and Buseck, 1989; Cabri et al., 1989; Miser and Buseck, 1991) to investigate the occurrence of precious metals in sulfide minerals. The distributions of precious metals in sulfides, such as Ag in galena, are of importance for understanding how foreign atoms are accommodated in sulfides and for maximizing recovery during ore processing (Cabri, 1987; Cabri et al., 1985). The Ag-bearing sulfides are complex, and the distribution of Ag between microscopic inclusions and PbS solid solutions is of fundamental importance. Concentrations of Ag coupled with Sb and Bi in galena have been investigated using high-sensitivity analytical techniques such as proton-induced X-ray emission (PIXE) (Cabri et al., 1984, 1985) and secondary ion mass spectrometry (SIMS) (Chryssoulis et al., 1986; McIntyre et al., 1984),

but little has been done using high spatial resolution techniques to distinguish apparent solid solution from microscopic inclusions.

STM is a powerful technique for investigating the atomic structure and morphology of semiconducting surfaces because it provides quantitative, real-space, atom-resolved images on the subnanometer scale as well as topographic images on the scale of about 10 to 10<sup>3</sup> nanometers. Because of the high resolution ( $\approx 0.02$  nm) in the *z* direction available with STM, even low-magnification images provide morphological information that is not attainable by methods such as scanning electron microscopy (SEM). High-magnification images show the topography of electronic states involved in the tunneling process. Under such conditions the image corresponds to a surface of constant local density of states (LDOS), which reflects the positions of surface atoms ( Tersoff and Hamann, 1985). Real-space imaging allows observation of individual defects such as steps, dislocations (Zheng et al., 1988; Cotterill and Bartlett, 1990), vacancies, and substitutional defects on surfaces (Hammers, 1988; Hammers and Demuth, 1988). Interpretation of defects is complicated by the fact that the electronic structure may differ significantly from that of the defect-free surface,

\* Present address: Department of Physics, Rice University, Houston, Texas 77251, U.S.A.

making the distinction between electronic and geometric effects difficult (Tersoff and Hamann, 1985).

### EXPERIMENTAL METHODS AND SAMPLE DESCRIPTIONS

STM experiments were conducted in a vacuum-compatible tunneling microscope to achieve atomic resolution of substitutional defects. W tips were made by electrochemical etching in 1 M KOH. Galena samples were cleaved in air and immediately loaded into the vacuum chamber, which was evacuated to a pressure  $<10^{-5}$  torr within 30 min of cleaving. Imaging was conducted at pressures  $<10^{-7}$  torr from 12 h to several days after cleaving. Images were collected after scanning for a sufficiently long time to eliminate tip instabilities.

Previous studies of O-exposed {100} surfaces of galena indicate that they are relatively inert with respect to oxidation (Hagstrom and Fahlman, 1978; Grandke and Cardona, 1980). Exposures of galena {100} surfaces to  $10^{12}$  Langmuirs of  $O_2$  (1 Langmuir equals  $10^{-6}$  torrs) resulted in only physisorption of  $O_2$ , so we believe that oxidation of our samples during their 30-min exposure to air is insignificant. Moreover, physisorption of  $O_2$  on galena {100} surfaces is reversible (Grandke and Cardona, 1980), and therefore most adsorbed  $O_2$  was probably removed in the vacuum before we imaged the surface. Although molecules other than  $O_2$  may have been adsorbed on our samples, previous STM studies of galena imaged in air and silicone oil (Hochella et al., 1989; Eggleston and Hochella, 1990) suggest that other adsorbates such as  $CO_2$  and  $H_2O$ , as well as silicone oil, do not affect the structure of galena {100} surfaces.

Galena has the NaCl structure, with perfect {100} cleavage and cell parameter  $a = 0.594$  nm. The unit mesh of a {100} surface is face centered, with Pb located at (0,0) and (1/2,1/2) and S atoms at (1/2,0) and (0,1/2). The separation between Pb and S atoms on a {100} surface is 0.297 nm, and that between Pb (or S) atoms is 0.424 nm. Imaging pure PbS in vacuum with a tip bias of  $-500$  mV has produced images where both atom species were resolved (Zheng et al., 1988). In these images one of the species protrudes from the surface more than the other. Based on the greater charge density for anions in Pb chalcogenides (Dalven, 1973), the protruding species were interpreted as  $S^{2-}$  anions (Zheng et al., 1988). STM of galena {100} surfaces in air and silicone oil has produced images showing half the atoms or all the surface atoms, depending on sample bias (Eggleston and Hochella, 1990). Using bias dependence and electronic structure, they concluded that S species are preferentially imaged with a high positive tip bias, whereas images with both atoms are produced with negative or low positive tip bias. With these results in mind, we would expect to see both S and Pb in our atomic-resolution images.

Samples of Ag-bearing galena from the Zacatecas mine in Mexico were chosen for study because they contain significant Ag concentrations and consist of large crystals (up to 2 cm). Large crystals were needed to make cleavage

fragments ( $>6$  mm wide) that could be easily clamped in our sample holder. Backscattered electron imaging of these samples showed many Ag-bearing inclusions. Electron microprobe analyses of the inclusion-free galena indicate variable concentrations of Ag and Sb, ranging from 0 up to 0.51 and 0.69 wt%, respectively, with average values of 0.16 and 0.24 wt%. Although substitution of  $Ag^+$  for  $Pb^{2+}$  is usually coupled with that of  $Sb^{3+}$  or  $Bi^{3+}$ , there is only a weak positive correlation between the Ag and Sb concentrations, and there is no detectable Bi in these samples. Sb is generally more concentrated than Ag, suggesting that there are additional defects, such as Pb vacancies, that maintain charge balance.

### STM IMAGES

#### Surface morphology

Cleaved {100} surfaces of Ag-bearing galena, like those of Ag-free samples examined in previous studies (Zheng et al., 1988; Hochella et al., 1989), are not atomically flat over large areas. Instead, the morphologies of cleavage surfaces are complex, reflecting the effects of defects on the cleavage process. In Ag-bearing galena flat regions occur on some surfaces, but they are usually associated with steps (4.5-nm steps in Fig. 1). The Ag-bearing samples also have surface pits ranging from 10 to 300 nm in diameter that are surrounded by topographically high regions (Fig. 1). These pits have a variety of shapes, with depths greater than 30 nm. Probing such narrow pits is limited by the tip geometry, so only a minimum depth could be determined.

HRTEM images indicate that rod-shaped inclusions of diaphorite ( $Pb_2Ag_3Sb_3S_8$ ) occur throughout the samples, ranging in diameter from tens to hundreds of nanometers (Sharp and Buseck, 1989). A possible explanation for the surface pits is that they were left behind where inclusions were plucked during cleavage. The rough areas around the pits appear to be accumulations of debris from plucking.

#### Surface structure

Most of the atomic-resolution images of the Ag-bearing samples have 0.42-nm corrugations (Figs. 2, 3a), indicating that only half of the atoms in the structure contribute to the image. Based on previous STM studies (referenced above) and charge density of bulk PbS samples (Dalven, 1973), these species are probably S atoms. Images showing all the surface atoms were also observed on these samples. Both types of images were obtained on the same sample with the same tip bias and tunnel current, suggesting that changes in tip structure as well as bias can play a significant role in the atomic-resolution imaging of galena. Such tip-surface interactions have been proposed to explain anomalous resolution and corrugation amplitudes on close-packed metal surfaces (Zheng and Tsong, 1990).

The atomic-resolution images of Ag-bearing galena indicate kinks in the atomic rows that parallel the [110]

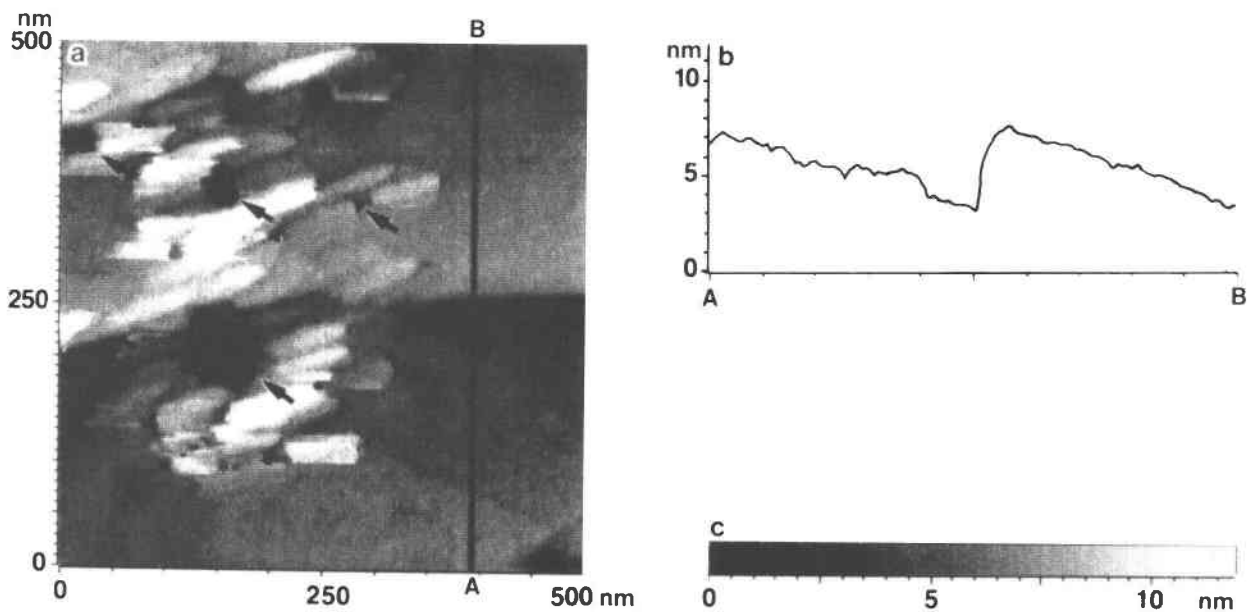


Fig. 1. Low-magnification STM image of (a) a galena (001) cleavage surface and (b) a cross section along line A-B showing cleavage-related morphology. The relief, represented by (c) the gray scale, is 11 nm. A 4.5-nm step, clearly evident in the cross section, runs across the center of the image (a). Also present are deep (>30-nm) pits (arrows) that are surrounded by rough regions that appear to consist of mineral fragments.

direction on the surface (Figs. 2, 3a), reflecting lateral displacements of the surface atoms from their ideal positions. A region of sample displayed the kinks during many scans of the area using different scan rates and imaging modes, indicating that the kinks are not artifacts of the scanning conditions. The images presented here (Figs. 2, 3a) were taken in constant-height mode using a relatively high scanning frequency of 50 Hz to minimize sample drift. Such drift, which results in a distortion of the entire image, does not cause local distortions, so we conclude that the observed kinks in Figures 2 and 3a are not the result of sample drift. The offsets in [110] rows

are aligned along [010] (Fig. 3a) forming bands that are one unit-cell wide and at least five cells long. The bands display smearing of the peaks along [110] and lower corrugation amplitudes (Fig. 2), possibly caused by different atomic species and a local difference in the surface LDOS.

The interpretations presented here are based on a limited number of observations and so are tentative, subject to additional atomic-resolution imaging. The bands of displaced surface atoms are interpreted as regions of strain, either localized at the surface or from defects intersecting the surface. Similar defects have not been reported in previous STM studies of galena. The defect surface (Fig. 3a) is compared to a Ag- and defect-free galena surface (Fig. 3b) to further illustrate the kinked rows. The Ag-free image (from Zheng et al., 1988) was collected on a very similar STM system with cleaving and imaging conditions nearly identical to those used in the present study. Surface defects that were observed on Ag-free galena were interpreted in terms of dislocations intersecting the cleavage surface (Zheng et al., 1988). In the Ag-bearing galena there is no indication of atomic steps or rows terminating at the defects, presumably ruling out dislocations as the source of the surface displacements.

Surface-atom displacements may result from Ag and Sb substitution for Pb. Although the concentrations of Ag and Sb are not generally equal, most analyses indicate the presence of both species. The ionic radius of  $\text{Ag}^+$  (0.129 nm) nearly equals that of  $\text{Pb}^{2+}$  (0.130 nm), but that of  $\text{Sb}^{3+}$  (0.090 nm) is much smaller and would result in significant local distortion where substituted for  $\text{Pb}^{2+}$  (ionic radii from Shannon, 1976). If substitution of  $\text{Ag}^+$  and  $\text{Sb}^{3+}$  occurs in groups, there would likely be distur-

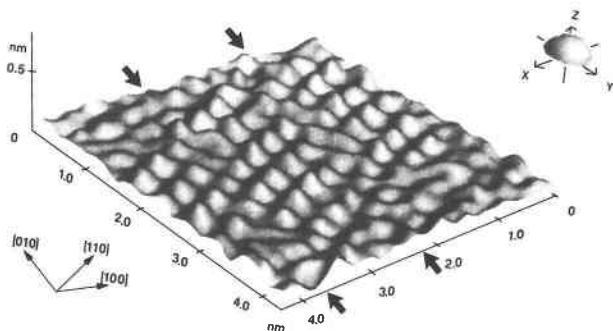


Fig. 2. Three-dimensional atomic-resolution image of a galena (001) surface showing peaks separated by 0.42 nm, probably corresponding to S atoms. This image is displayed as a three-dimensional surface with oblique illumination, as illustrated in the upper-right corner. Viewing the surface along [110] shows that the rows of atoms are kinked. The kinks are aligned along [010] (between arrows) into bands that have low corrugation amplitudes and a smeared appearance.

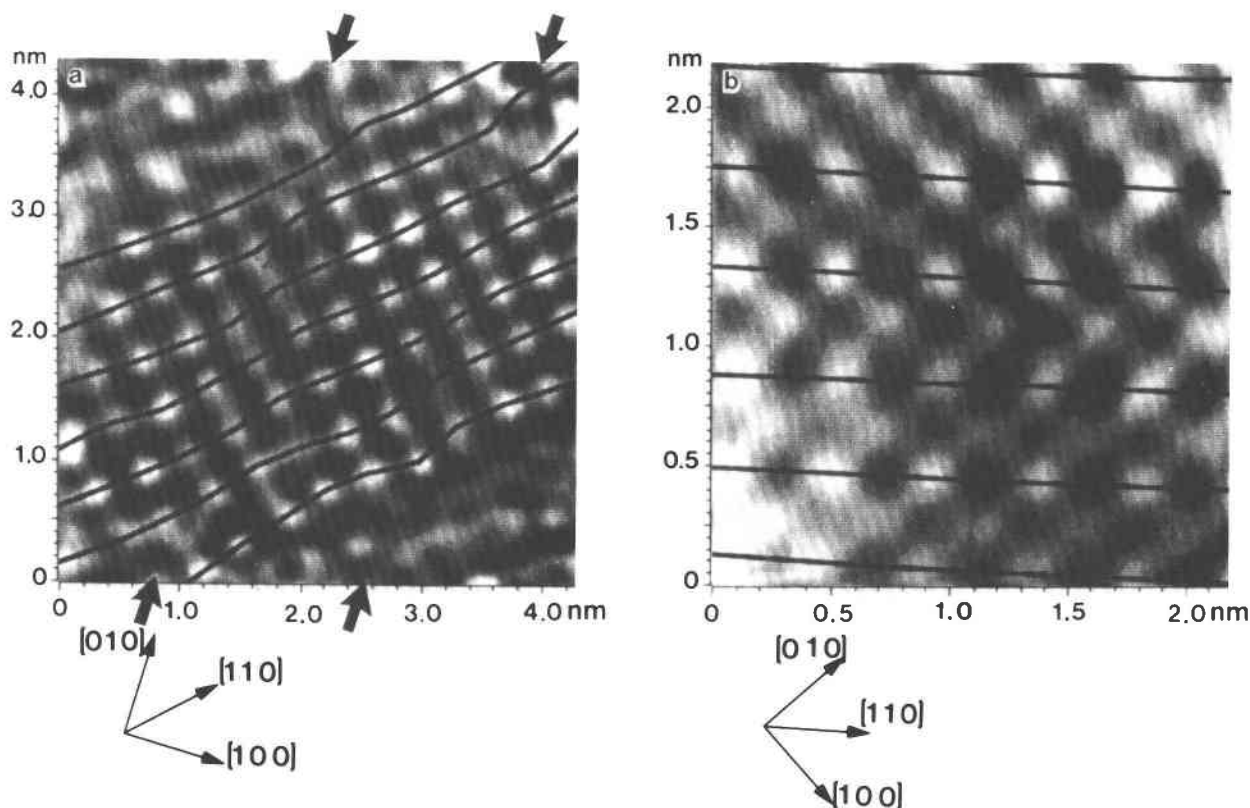


Fig. 3. Gray-scale images of (a) Ag-bearing galena (4.3 nm  $\times$  4.3 nm) and (b) Ag-free galena (2.2 nm  $\times$  2.2 nm). The image of Ag-bearing galena has 0.42-nm atomic separations indicating only S atoms contributing to the image, whereas the Ag-free galena has 0.30-nm atomic separations indicating both the S atoms (rows of light spots highlighted by dark lines) and the Pb atoms (rows of light spots between the dark lines). In both images the rows of S atoms along [110] are highlighted with dark lines, illustrating the kinks in the Ag-bearing galena. These kinks occur along bands of smeared structure that parallel [010] (between the arrows).

tion over many unit cells. The displacements of atoms seen in STM images could be the surface expression of such distortion.

Substitution of  $\text{Ag}^+$  and  $\text{Sb}^{3+}$  for  $\text{Pb}^{2+}$  would also result in local distortions of the electronic structure. In addition to the differences in charge,  $\text{Ag}^+$   $[(\text{Kr})4d^{10}]$  has two fewer valence electrons than  $\text{Pb}^{2+}$   $[(\text{Xe})4f^{14}5d^{10}6s^2]$  or  $\text{Sb}^{3+}$   $[(\text{Kr})4d^{10}5s^2]$  to contribute to the valence band, thereby changing the LDOS. Because atomic-resolution images are dependent on the surface LDOS ( Tersoff and Hamann, 1985), the distortion in STM images could be the result of electronic variations as well as strain. While the STM images in the present work can be interpreted as evidence for grouped substitution of  $\text{Ag}^+$  and  $\text{Sb}^{3+}$  in galena, further evidence will be provided by additional imaging and planned experiments of scanning tunneling spectroscopy where the electronic structure and possibly the atomic species at defects can be identified.

### CONCLUSIONS

Ag-bearing galena has surface morphological and structural features that differ from those of Ag-free galena. Pits, surrounded by what appear to be crystal fragments, are interpreted as resulting from the plucking of diapho-

rite inclusions during cleavage. Atomic-resolution images indicate local distortions of the surface structure that may be the result of  $\text{Ag}^+$  and  $\text{Sb}^{3+}$  substitution for  $\text{Pb}^{2+}$ .

### ACKNOWLEDGMENTS

We thank C.S. Chang for assistance with STM experiments, James Clark for assistance with the electron microprobe analyses, and Don Burt and Mike Sheridan for the samples. We also thank Grant Henderson and an anonymous referee for reviewing the manuscript, as well as Simon Peacock and Stuart Lindsay for helpful discussions. The electron microprobe facility is funded by NSF grant EAR-8408529. This work was funded by NSF grant EAR-8708529.

### REFERENCES CITED

- Cabri, L.J. (1987) The mineralogy of precious metals: New developments and metallurgical implications. *Canadian Mineralogist*, 25, 1–7.
- Cabri, L.J., Campbell, J.L., Lafamme, J.H.G., Leigh, R.G., Maxwell, J.A., and Scott, J.D. (1985) Proton-microprobe analysis of trace elements in sulfides from some massive sulfide deposits. *Canadian Mineralogist*, 23, 133–148.
- Cabri, L.J., Chrystoulis, S.L., De Villiers, J.P.R., Lafamme, J.H.G., and Buseck, P.R. (1989) The nature of "invisible" gold in arsenopyrite. *Canadian Mineralogist*, 27, 353–362.
- Cabri, L.J., Harris, D.C., and Nobling, R. (1984) Trace silver analysis by proton microprobe in ore evaluation. In U. Kudryk, D.A. Corrigan, and W.W. Liang, Eds., *Precious metals: Mining, extraction, and processing*, Proceedings of the Metallurgical Society of AIME, p. 93–100.
- Chrystoulis, S.L., Chauvin, W.J., and Surges, L.J. (1986) Trace element

- analysis by secondary ion mass spectrometry with particular reference to silver in Brunswick sphalerite. *Canadian Mineralogist*, 25, 233–239.
- Cotterill, G.F., Bartlett, R., Hughes, A.E., and Sexton, B.A. (1990) STM investigations of galena surfaces in air. *Surface Science Letters*, 232, L211–L214.
- Dalven, R. (1973) Electronic structure of PbS, PbSe, and PbTe. In H. Ehrenreich, F. Seitz, and D. Turnbull, Eds., *Solid State Physics*, vol. 28, p. 179–224. Academic Press, New York.
- Eggleston, C.M., and Hochella, M.F., Jr. (1990) Scanning tunneling microscopy of sulfide surfaces. *Geochimica et Cosmochimica Acta*, 54, 1511–1517.
- Grandke, T., and Cardona, M. (1980) Electronic properties of clean and oxygen covered (100) cleaved surfaces of PbS. *Surface Science*, 92, 385–392.
- Hagstrom, A.L., and Fahlman, A. (1978) The interaction between oxygen and the lead chalcogenides at room temperature studied by photoelectron spectroscopy. *Applied Surface Science*, 1, 455–470.
- Hammers, R.J. (1988) Characterization of localized atomic surface defects by tunneling microscopy and spectroscopy. *Journal of Vacuum Technology*, B6, 1462–1467.
- Hammers, R.J., and Demuth, J.E. (1988) Electronic structure of localized Si dangling-bond defects by tunneling spectroscopy. *Physical Review Letters*, 60, 2527–2530.
- Hochella, M.F., Jr., Eggleston, C.H., Elings, V.B., Parks, G.A., Brown, G.E., Jr., Wu, C.M., and Kjoller, K. (1989) Mineralogy in two dimensions: Scanning tunneling microscopy of semiconducting minerals with implications for geochemical reactivity. *American Mineralogist*, 74, 1233–1246.
- McIntyre, N.S., Cabri, L.J., Chauvin, W.J., and Laflamme, J.H.G. (1984) Secondary ion mass spectrometry study of dissolved silver and indium in sulfide minerals. *Scanning Electron Microscopy* 3, 1139–1147.
- Miser, D.E., and Buseck, P.R. (1991) Defect microstructures in a gold-bearing arsenopyrite. *Canadian Mineralogist*, in press.
- Shannon, R.D. (1976) Revised effective ionic radii and systematic studies of interatomic distances in halides and chalcogenides. *Acta Crystallographica*, A32, 751–767.
- Sharp, T.G., and Buseck, P.R. (1989) Distribution of silver in galena: A high spatial resolution study. *Geological Society of America Abstracts with Programs*, 21-6, A248.
- Sharp, T.G., Zheng, N.J., Chang, C.S., Tsong, I.S.T., and Buseck, P.R. (1989) Scanning tunneling microscopy studies of galena (001) cleavage surfaces. *Eos*, 70-43, 1394.
- Tersoff, J., and Hamann, D.R. (1985) Theory of the scanning tunneling microscope. *Physical Review*, B31, 805–813.
- Zheng, N.J., and Tsong, I.S.T. (1990) Resonant-tunneling theory of imaging close-packed metal surfaces by scanning tunneling microscopy. *Physical Review*, B41, 2671–2677.
- Zheng, N.J., Wilson, I.H., Knipping, U., Burt, D.M., Krinsley, D.H., and Tsong, I.S.T. (1988) Atomically resolved scanning tunneling microscopy images of dislocations. *Physical Review*, B38, 12780–12782.

MANUSCRIPT RECEIVED AUGUST 29, 1990

MANUSCRIPT ACCEPTED NOVEMBER 7, 1990